The Electrical Conductivity of Methylene-Methyliminomethyl Formamidine Molecular Nanowire via DFT and QTAIM theory

S. Palanisamy[1] and K. Selvaraju[1]*

[1, 1*] Department of Physics, Kandaswami Kandar's College, Velur-638182, Namakkal (Dt,) India

* Corresponding author: physicsselvaraj@gmail.com

A B S T R A C T

The effect of metal electrodes on methylene-methyliminomethyl formamidine (MMF) molecule has been calculated by Density functional analysis using Gaussian09 program package. The various applied electric fields $(0.00 - 0.26 \, V\text{Å}^{-1})$ altered the geometrical parameters and the corresponding electrostatic and transport properties of the molecule has been analyzed. The variations in the atomic charges (MPA, NPA) of the molecule for the various applied electric fields have been compared. The HOMO-LUMO gap of the molecule for zero bias is 1.904 eV, as the field increases this gap decreases to 0.272 eV. The ESP shows the potential difference between charges accumulated of the molecule for various applied electric fields. The applied electric field polarizes the molecule, in consequence of that the dipole moment of the molecule decreases from 9.65 to 8.82 Debye. The small decrease of dipole moment shows that the molecule exhibits smaller conductivity.

Keywords: Nano wire, DFT, HLG, ESP, Dipole moment, I-V

I. INTRODUCTION

The electron transport on the molecules with chains of alkane happens through tunneling mechanism. When the molecules with alkane chains were sandwiched between the electrodes, the result will be exponential increase of the junction resistance [1]. The higher energy band gap (~6 eV) aids the insulating nature of the molecules and hence can be performed as insulators [2]. The studies on the electron transport and conductance of ethane, butane, octane and n-alkane dithiols have been recently reported [3-5]. The current methodology incorporated a detailed study to analyse the electron transport properties of long methylene formamide chain molecule; methylene - methyliminomethyl formamidine (MMF) also expressed as MMF with chemical formula $C_4N_3H_5$. The structural analysis of MMF indicated the presence of a chain of 3 carbon atoms alternatively attached to N atoms along with a

methylene group attached in the terminal end. Each carbon atoms in the chain were found to be attached with hydrogen atoms satisfying the valance. The current study also aimed to resolve the effect of external electric field (EF) on Au and S substituted MMF where the Au atom operates as electrode and S atom being the linker figure 1. The response of the applied external electric field over the structural, bond topological at bcp and electrostatic properties of the molecule were studied in detail in the current research.
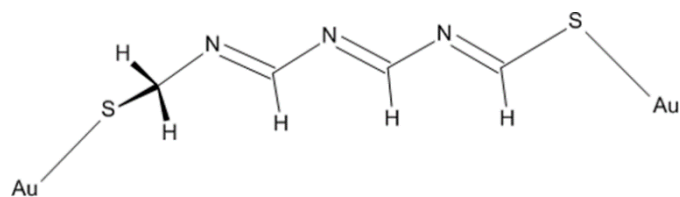

Figure 1. Au and S substituted methylene-methyliminomethylformamidine (MMF) molecule.

II. COMPUTATIONAL METHODOLOGY

The gold and sulpher attached MMF system ($C_4N_3H_5S_2Au_2$) was geometrically minimized for the zero and higher applied electric fields with five field steps within the range of $\pm 0.26 V\text{Å}^{-1}$ using density functional method [6] incorporated in Gaussian09 program package [7]. For the optimization, permutation of Becke's three- parameter exchange function with non-local correlation of Lee, Yang and Parr (B3LYP hybrid function) [8] is used along with Los Alamos National Laboratory of double zeta basis set [LANL2DZ], as it delivers the complete explanation of heavy metal atoms [9] in the MMF molecular wire. The MPA charges were calculated with polarization and diffuse functions. In this computation, the Vander Waals radius of gold and sulpher atom has been encompassed in the input file. The structural energy minimization were evaluated by through Berny algorithm and the optimization is converged with the threshold value of 0.00045, 0.0003, 0.0018 and 0.0012au for the maximum force, root mean square force (RMS), maximum displacement and RMS displacement respectively. The
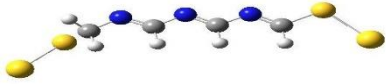
self-consistency of the non-interactive wave function is performed with the requested convergence on the density matrix of 10^{-8} and 10^{-6} for the RMS and maximum density matrix error between the iterations. In this chapter, all the quantum computation were carried out for different levels of applied electric field to analyse the variations in the geometry conformation, chemical bond characteristics and the electrostatic potential of the MMF molecule. The bond topological and the electrostatic properties have been predicted from the QTAIM theory [10] via EXT94b module implemented in the AIMPAC software [11]. The graphical program packages DENPROP [12] and wfn2plots/XD [13] were used to generate 2D/3D grid for plotting Laplacian of charge density and the deformation density maps. The three dimensional surface plots of frontier molecular orbitals and electrostatic potential were posed from GVIEW05 package [14]. Also, the density of states (DOS) at five different electric potential EFs was determined from GaussSum program [15].

III. RESULTS AND DISCUSSION

3.1 Geometry Aspects

The geometry minimized structure of gold and sulpher substituted MMF molecular wire for the zero and higher field was shown in the figure 2. The structural considerations such as bond distances, bond angles, and dihedral angles are the significant parameters in calculating the atomic properties of the molecules in electron level resolution. Still the molecule is found to be symmetric, feeble differences are noticed on the left and right side of the molecule. The dissimilarities in bond distances of the MMF molecular wire for the different applied electric field with reference to zero electric field are depicted in the figure 3. The average bond distances of C-N bonds, C(1)-N(1), C(2)-N(2) and C(3)-N(3) is 1.421 Å for zero electric field, whereas this distance is increased by the maximum of 0.01 Å when the field is increased from 0 eV. The C=N distances at the zero

field (1.295 Å) was getting decreased to 1.286 Å for the increasing applied field. The average distance of C–H bond is 1.102 Å which remains nearly similar for the higher electric field. The S–C bond length is found to be ~1.876 Å in the absence of electric potential, which agree well to the previously reported value [16-18]. In the left end the S–C bond lengths vary from 1.939 to 1.957 Å, while at the right end the variation ranges from 1.814 to 1.834 Å, when the field is increased from 0 to 0.26eV. Specifically, the geometry variations are found to be significant the terminal regions because of the weak interaction between the gold atom and the molecule. The maximum variation of 0.007 and 0.006 Å from Au-S bond length, ~2.388 Å is found to be noticed when the field is increased form 0 eV at both the left and right ends of the molecule. The N–C–S bond angle in the terminal side of the molecule for zero fields is 111.7° and 101.9° respectively. However, as the field rises, the left end (10.7°) is found to maximum when compared to the R-end (0.3°). The Au–S–C bond angle for the zero field at both the ends are ~101.9°; as the field increases, the variations are unequal. The zero field torsion angles of the terminal S(1)–C(1)–N(1)–C(2) bond is -107°, the bond twist is severely affected by the maximum of 110.4°; whereas the torsion angle for S(2)–C(4)–N(3)–C(3) varies from -177.3° to -178.1° (Table 1) with the minimum variation for the external potential. Thus the L-end of the molecular wire is highly responsive to the applied potential when compared to the R-end. Surprisingly, the Au–S–C–N bonds at both ends are twisted in opposite direction when the applied electric field is increased from 0 [-174.6°] to 0.26 VÅ⁻¹ [179.2°].
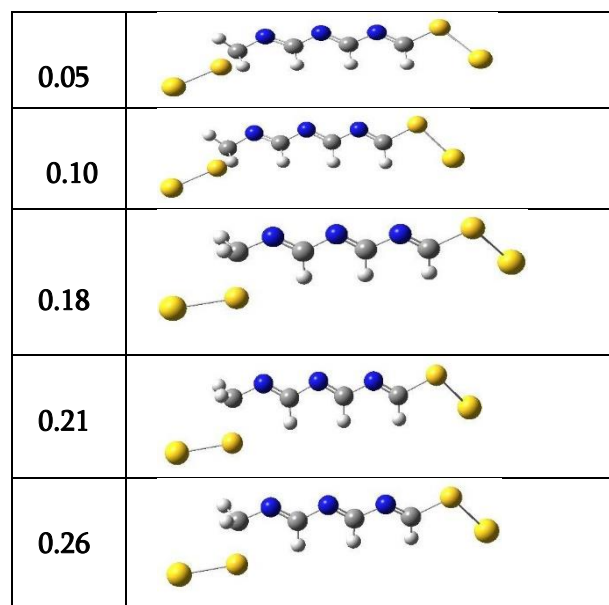

Figure 2. Optimized geometry of Au and S substituted MMF molecule for the zero and various applied EFs.
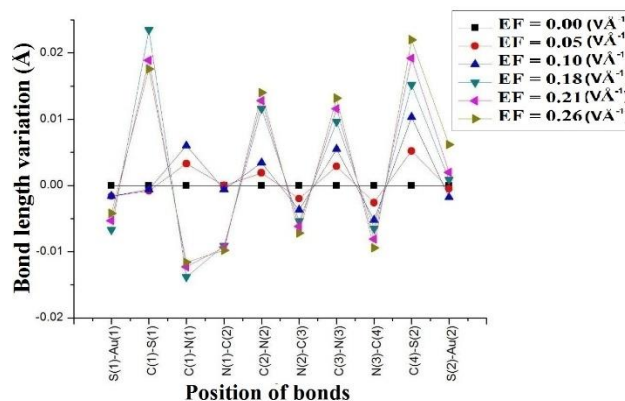

Figure 3. Showing bond length variations of Au and S substituted MMF for the various applied EFs.

Table 1. Geometrical parameters (Bond Length, Bond Angle and Torsion Angle) (Å, °) of Au and S substituted MMF molecule for the zero and various applied EFs.

EFs (VÅ⁻¹)	Optimized Geometry
0.00	

Bonds	Applied electric field (VÅ⁻¹)					
	0.00	0.05	0.10	0.18	0.21	0.26
C-N Bonds						
C(1)-N(1)	1.454	1.458	1.460	1.441	1.442	1.443
C(2)-	1.295	1.295	1.295	1.286	1.28	1.285

N(1)					6	
C(2)-N(2)	1.408	1.409	1.411	1.419	1.420	1.422
C(3)-N(2)	1.299	1.297	1.295	1.294	1.293	1.292
C(3)-N(3)	1.401	1.404	1.407	1.411	1.413	1.415
C(4)-N(3)	1.291	1.289	1.286	1.285	1.283	1.282
C-H Bonds						
C(1)-H(1A)	1.091	1.090	1.089	1.093	1.093	1.094
C(1)-H(1B)	1.100	1.100	1.099	1.093	1.093	1.093
C(2)-H(2)	1.112	1.111	1.110	1.104	1.103	1.103
C(3)-H(3)	1.112	1.111	1.110	1.110	1.109	1.109
C(4)-H(4)	1.097	1.097	1.097	1.097	1.096	1.096
Terminal Bonds						
S(1)-C(1)	1.939	1.938	1.939	1.963	1.958	1.957
S(2)-C(4)	1.814	1.819	1.824	1.829	1.833	1.836
Au(1)-S(1)	2.384	2.383	2.383	2.377	2.379	2.380
Au(2)-S(2)	2.392	2.391	2.390	2.392	2.394	2.398
Bond angles						
Terminal Bonds						
S(1)-C(1)-N(1)	105.4	105.6	106.0	116.0	116.1	116.1
S(2)-C(4)-N(3)	118.0	117.8	117.6	116.0	117.7	117.6
Au(1)-	101.3	101.6	101.7	116.0	100.	100.9

S(1)-C(1)					7	
Au(2)-S(2)-C(4)	102.5	102.3	102.2	116.0	101.4	101.4
Torsion Angles						
Terminal Bonds						
S(1)-C(1)-N(1)-C(2)	-107.0	-98.5	-91.6	116.0	2.8	3.3
S(2)-C(4)-N(3)-C(3)	179.4	179.7	178.2	116.0	-177.3	-179.4
Au(1)-S(1)-C(1)-N(1)	-170.8	-174.8	-174.6	116.0	-178.0	178.5
Au(2)-S(2)-C(4)-N(3)	-178.4	179.9	-175.7	116.0	-167.9	179.9

3.2 Topology of Electron density analysis

The two dimensional contour plot of deformed electron density of MMF molecule for the zero and non-zero bias was shown in the figure 4. The chemistry of the electron density distribution can be well exposed by means of deformation density, and its second derivative Laplacian of electron density and the electrostatic potential [19]. The topological analysis of electron density differentiates the electron density sharing of C–N, C=N, S–C and Au–S bonds in the molecules. The average value of C–N bond electron density $\rho_{bcp}(r)$ at the bond critical point is ~1.82 eÅ^{-3} for the zero applied electric field. This value is faintly smaller than the C=N bond densities which is ~2.33 eÅ^{-3}. Notably, the C-N bond densities are decreasing and C=N densities are increasing with the applied field. For the applied field (0.05 - 0.26 VÅ^{-1}), the variations of

C-N bond densities $\rho_{bcp}(r)$ are unequal and ranges from 1.673 to 1.882 eÅ^{-3}; whereas $\rho_{bcp}(r)$ for C=N bonds varies from 2.330 to 2.383 eÅ^{-3}.

EFs (VÅ^{-1})	Deformation density
0.00	
0.05	
0.10	
0.18	
0.21	
0.26	

Figure.4 Electron deformation density plot of MMF molecule for the different electric potential EFs.

Among the covalent bond in MMF molecular wire, the S–C bond electron density is feeble, which shows that the charges of these bonds at the bond critical point move away from the inter-nuclear axis, which approves its dominant π-bond characteristic. The similar scenario can be reflected from the Laplacian of electron density and the bond ellipticity at the bcp. In both the right and left ends, the electron densities at bcp of S–C bond density are ~0.956 eÅ^{-3} at the zero electric field. This bond density value is found to be decreases, when the field is increased from Zero eV and the extreme

difference in the left edge is 0.023 eÅ^{-3} while, in the right side, it is 0.037 eÅ^{-3}. Concerning the Au–S bond, the electron density in the both the ends are 0.535 and 0.536 eÅ^{-3} respectively for the zero bias; and these values are getting increased by 0.006 and 0.008 eÅ^{-3} respectively in the left and right ends when the field is increased from the zero bias. As expected the electron density for C-H bonds are found as ~1.751 eÅ^{-3}. An open-shell interaction in C–N and C=N bonds can be clearly revealed from the negative Laplacian of electron density values which authorizes the covalent character of these bonds. And the closed-shell type of interactions in Au–S bonds is well confirmed from the positive Laplacian of electron. Also, it is determined that the charges scattered well in these bond regions, and the same can be pictured from the Laplacian of electron density contour plots (Fig. 5) for the zero and higher applied electric fields. The Laplacian of electron density diverges expressively merely in the right and left edge bonds. For the Au–S bond in the left end, the $\nabla^2\rho_{bcp}(r)$ values differs from 2.9 to 3.2 eÅ^{-5}, while in the right edge, the variation ranges from 3.1 to 2.9 eÅ^{-5} when the field is escalated from 0 to 0.26 VÅ^{-1}. The complete variation in $\rho_{bcp}(r)$ and $\nabla^2\rho_{bcp}(r)$ for zero and non-zero bias was clearly plotted in the figure 6 and the corresponding values are listed in the Table 3.
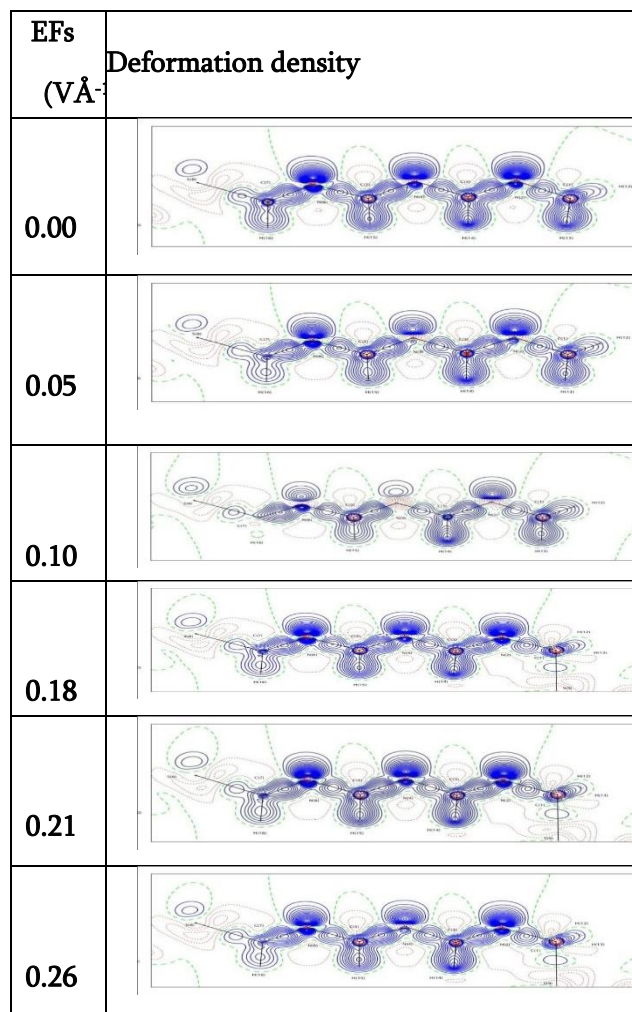
Table 2. Electron density ρ_{bcp} (r) (eÅ^{-3}) values of Au and S substituted MMF molecule for the zero and various applied EFs (VÅ^{-1}).

Bonds	Applied electric field (VÅ^{-1})					
	0.00	0.05	0.10	0.18	0.21	0.26
C-N Bonds						
C(1)-N(1)	1.699	1.685	1.673	1.705	1.698	1.695
C(2)-N(1)	2.330	2.334	2.340	2.339	2.342	2.345
C(2)-N(2)	1.878	1.868	1.858	1.826	1.818	1.811
C(3)-N(2)	2.325	2.333	2.338	2.350	2.353	2.358
C(3)-N(3)	1.882	1.866	1.851	1.833	1.822	1.813
C(4)-N(3)	2.343	2.354	2.363	2.371	2.377	2.383
C-H						

| bonds						
C(1)-H(1A)	1.809	1.815	1.820	1.787	1.785	1.784
C(1)-H(1B)	1.759	1.760	1.763	1.791	1.789	1.790
C(2)-H(2)	1.711	1.713	1.717	1.749	1.751	1.752
C(3)-H(3)	1.713	1.715	1.718	1.721	1.722	1.722
C(4)-H(4)	1.764	1.764	1.765	1.764	1.764	1.764
Terminal Bonds						
S(1)-C(1)	0.853	0.853	0.851	0.823	0.830	0.832
S(2)-C(4)	1.060	1.052	1.043	1.035	1.028	1.023
Au(1)-S(1)	0.535	0.537	0.537	0.542	0.541	0.541
Au(2)-S(2)	0.536	0.536	0.536	0.533	0.531	0.528

EFs (VÅ^{-1})	Laplacian of electron density
0.00	
0.05	
0.10	
0.18	
0.21	
0.26	
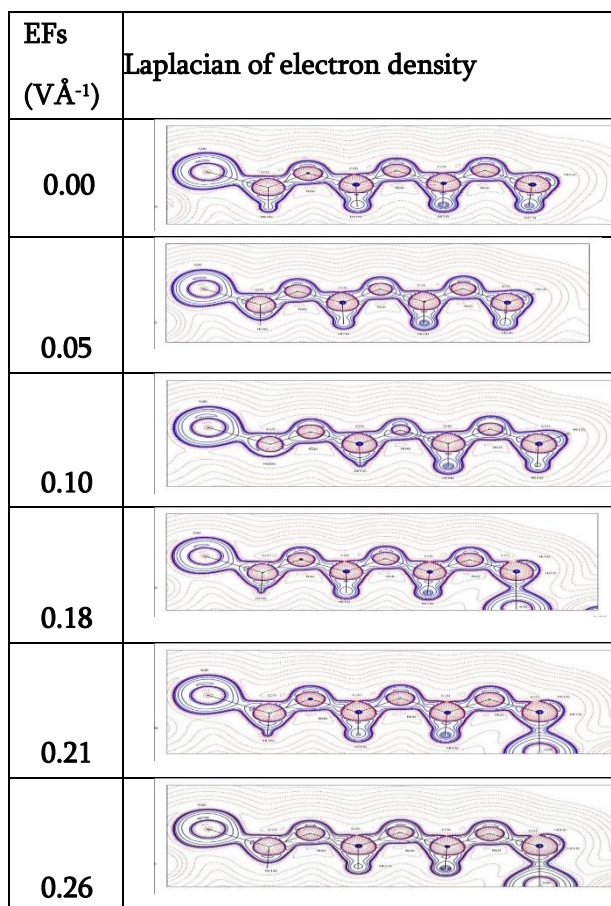
Figure 5. The contour plot of Laplacian of electron density maps of MMF molecule for different electric potential EFs.
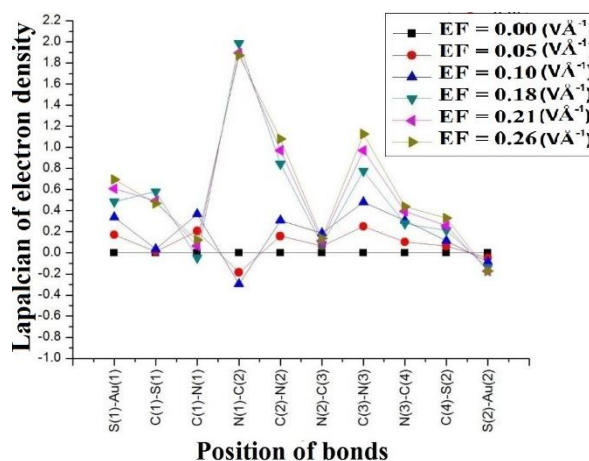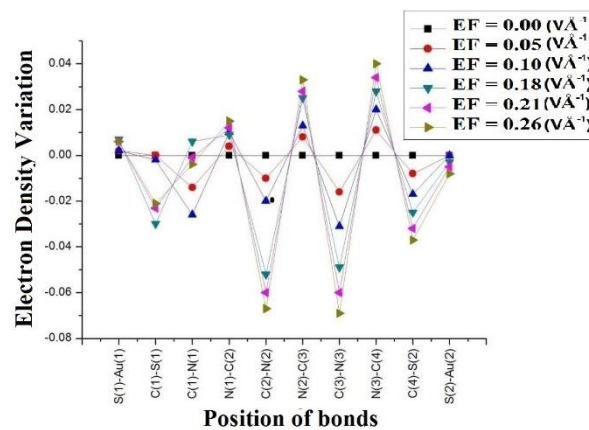
Figure 6. The deviations of Electron density and Laplacian of electron density of MMF molecule for the different electric potential.

Table 3 Laplacian of electron density of MMF for the zero and non-zero electricfields (VÅ^{-1}).

Bonds	Applied electric field (VÅ^{-1})					
	0.00	0.05	0.10	0.18	0.21	0.26
C-N Bonds						
C(1)-N(1)	-11.415	-11.208	-11.046	-11.463	-11.348	-11.293
C(2)-N(1)	-18.196	-18.381	-18.492	-16.212	-16.302	-16.323
C(2)-N(2)	-14.316	-14.157	-14.01	-13.47	-13.3	-13.2

			0	3	43	36
C(3)-N(2)	-19.000	-18.933	-18.815	-18.920	-18.884	-18.862
C(3)-N(3)	-14.336	-14.085	-13.854	-13.560	-13.366	-13.209
C(4)-N(3)	-18.251	-18.147	-17.943	-17.974	-17.857	-17.812
C-H bonds						
C(1)-H(1A)	-21.047	-21.234	-21.403	-20.633	-20.629	-20.637
C(1)-H(1B)	-19.240	-19.284	-19.376	-20.724	-20.728	-20.775
C(2)-H(2)	-18.068	-18.140	-18.249	-19.278	-19.338	-19.372
C(3)-H(3)	-18.148	-18.196	-18.300	-18.367	-18.403	-18.404
C(4)-H(4)	-19.897	-19.885	-19.902	-19.888	-19.870	-19.877
Terminal Bonds						
S(1)-C(1)	-1.951	-1.936	-1.914	-1.370	-1.458	-1.481
S(2)-C(4)	-4.645	-4.473	-4.307	-4.161	-4.037	-3.950
Au(1)-S(1)	2.868	2.933	2.984	3.080	3.126	3.199
Au(2)-S(2)	3.082	3.033	2.996	2.943	2.909	2.910

3.3 Bond energy distribution

Chemical interactions were also carried out from energy density and electrostatic concepts of chemical bonds. In this chapter, the total energy density distribution of MMF molecule has been predicted, which is associated with the second derivative of electron density. The positive $\nabla^2 \rho_{bcp}(r)$ results the influence of the kinetic energy density results the exhaustion of charges at the bond critical point; whereas the negative Laplacian represents the governance of potential energy density, and the concentration of charges [20]. The total energy density H(r) from potential energy density V(**r**) and the local kinetic energy density G(**r**) in the bonding region can be equated as H(**r**) = G(**r**) + V(**r**).

Relatively, the high negative ($\sim$-1.755/-3.094 HÅ^{-3}) total energy density H(**r**) for the C–N and C=N bonds are noticed when compared with that of C-H, S-C and Au-S bonds. Conversely, a small deviation is found to be predicted with the field escalation from 0 eV. The total energy density of C-H bonds are found to be high and the values are $\sim$ -1.633 HÅ^{-3} for zero basis condition and there is no significant difference was noticed when the field is increased from zero bias. The same scenario was replicated in S-C bonds, in which the values were decreased from -0.396 to -0.369 HÅ^{-3} for the L-end and for the R-end, varies from -0.681 to -0.608 HÅ^{-3}. The Au(1)-S(1) bond, the energy density is almost equal, the value is -0.167 HÅ^{-3}, whereas in Au(2)-S(2) bond the value vary from -0.161 to -0.165 HÅ^{-3}. Table-4 lists the computed values of total energy density of the MMF molecule. The complete variation of the total energy density of the MMF molecule for the zero and higher electric fields is shown in figure 7. On the whole, it is noticed that the total energy density H(r) differences are asymmetric in the terminal bonds at right and left ends of the molecule.
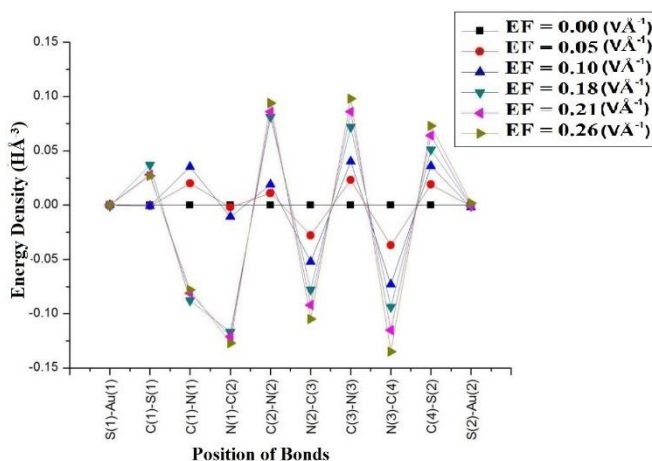
Figure. 7 Energy density variations of Au and S substituted MMF for the zero andvarious applied EFs.

Table 4. Total energy density distribution (HÅ^{-3}) for the zero and higher electric fields (VÅ^{-1}).

Bonds	Applied electric field (VÅ^{-1})					
	0.00	0.05	0.10	0.18	0.21	0.26
C-N Bonds						
C(1)-N(1)	1.515	1.495	1.480	1.603	1.596	1.593
C(2)-N(1)	3.103	3.105	3.114	3.220	3.224	3.230
C(2)-N(2)	1.855	1.844	1.836	1.774	1.769	1.761
C(3)-N(2)	3.041	3.069	3.093	3.119	3.133	3.146
C(3)-N(3)	1.896	1.873	1.856	1.824	1.810	1.798
C(4)-N(3)	3.139	3.176	3.212	3.233	3.254	3.274
C-H bonds						
C(1)-H(1A)	1.749	1.762	1.771	1.717	1.716	1.714
C(1)-H(1B)	1.643	1.645	1.651	1.723	1.723	1.725
C(2)-H(2)	1.550	1.555	1.562	1.631	1.636	1.638
C(3)-H(3)	1.554	1.558	1.565	1.570	1.573	1.573
C(4)-H(4)	1.672	1.672	1.673	1.673	1.673	1.673
Terminal Bonds						
S(1)-C(1)	0.396	0.397	0.397	0.359	0.368	0.369
S(2)-C(4)	0.681	0.662	0.645	0.630	0.617	0.608
Au(1)-S(1)	0.167	0.167	0.167	0.168	0.167	0.167
Au(2)-S(2)	0.163	0.164	0.165	0.164	0.164	0.161

3.4 Atomic charges

To evaluate the conductivity performance of a molecular wire, the analysis over the charge distribution of atoms is mandatory. It is vital study the charge redistribution of molecules under applied electric field to investigate all the charges associated molecular properties. In this chapter, the point charges derived from the two anticipated procedures (i) based on wave functions and (ii) based on fitting of molecular electrostatic potential, MESP, have been computed [21]. Meanwhile different algorithms implement different methodology over the charge calculation; it is a preliminary factor to calculate the electronic charges from various algorithms. Presently, the charge distribution for zero and higher bias, listed in Table5, determined by electrostatic potential fitting methods, which was compared against the natural population analysis (NPA) charges [22]. Amongst charges calculated from NPA scheme are superior pattern.

The NPA charges of carbon atoms, which are associated to the N and S atoms exhibits high positive charge, 0.211e. This could be the main consequence of heavy atoms attached at right and left ends of the molecule, MPA charges of the corresponding atoms are seems highly negative, ~ -0.351e. The NPA charges of S-atom on left end of the wire for zero bias is highly negative ~ -0.206e; as the field increases, in the left end, this value increases to -0.349e; whereas in the right end, the value

increases from -0.071 to -0.091e. The NPA charges of Au(1) atom found to increase from 0.227 to 0.357e, when the field increased from zero bias. Remarkably, the charge of right end Au atom gradually decreases from 0.292 to 0.162 e for the applied electric field increased from 0 to 0.26 VÅ^{-1}. Interestingly, systematic charge variation is observed in both right and left end of the MMF molecular wire.

Table. 5 Atomic charges (e) of MMF molecule for the applied electric potential (VÅ^{-1})
(first line MPA charges, second line NPA charges).

Atoms	Applied electric field (VÅ^{-1})					
	0.00	0.05	0.10	0.18	0.21	0.26
C(1)	-0.572	-0.579	-0.584	-0.584	-0.565	-0.566
	-0.297	-0.300	-0.302	-0.302	-0.300	-0.300
C(2)	-0.245	-0.247	-0.248	-0.248	-0.280	-0.281
	0.271	0.264	0.259	0.259	0.242	0.242
C(3)	-0.275	-0.279	-0.281	-0.281	-0.287	-0.289
	0.290	0.286	0.281	0.281	0.269	0.269
C(4)	-0.311	-0.310	-0.310	-0.310	-0.314	-0.308
	-0.013	-0.012	-0.010	-0.010	-0.011	-0.007
N(1)	0.042	0.045	0.047	0.047	0.077	0.079
	-0.450	-0.441	-0.434	-0.434	-0.402	-0.400
N(2)	0.068	0.072	0.075	0.075	0.074	0.074
	-0.450	-0.444	-0.437	-0.437	-0.426	-0.424
N(3)	0.075	0.076	0.077	0.077	0.082	0.079
	-0.497	-0.493	-0.488	-0.488	-0.479	-0.476
H(1A)	0.285	0.289	0.292	0.292	0.286	0.290
	0.244	0.246	0.247	0.247	0.255	0.258
H(1B)	0.215	0.220	0.225	0.225	0.286	0.289
	0.196	0.199	0.202	0.202	0.255	0.256
H(2)	0.170	0.173	0.178	0.178	0.209	0.211
	0.137	0.140	0.143	0.143	0.160	0.161
H(3)	0.176	0.178	0.183	0.183	0.186	0.187
	0.139	0.140	0.143	0.143	0.145	0.146
H(4)	0.227	0.226	0.228	0.228	0.228	0.228
	0.187	0.187	0.187	0.187	0.187	0.187
S(1)	0.070	0.053	0.038	0.038	-0.087	-0.085
	-0.206	-0.223	-0.240	-0.240	-0.367	-0.349
S(2)	0.138	0.134	0.128	0.128	0.115	0.108
	-0.071	-0.074	-0.080	-0.080	-0.091	-0.081
Au(1)	-0.062	-0.031	-0.008	-0.008	0.064	0.094
	0.227	0.254	0.276	0.276	0.348	0.357
Au(2)	0.000	-0.021	-0.039	-0.039	-0.076	-0.109
	0.292	0.272	0.253	0.253	0.215	0.162

3.5 Frontier Molecular orbital analysis

The electron transport characteristics [23] was well established from energy gap between the highest occupied molecular orbital (HOMO) and lowest unoccupied molecular orbital (LUMO).Thus it is essential to inspect the differences in HOMO-LUMO gap and molecular orbital energy levels for the different potential. Fig. 8 depicts the variation of HLG for the zero and non-zero basis of MMF molecular wire. The applied electric field significantly point out the frontier orbital energy levels (HOMO and LUMO) of the system, which are varied from each other and are predominantly
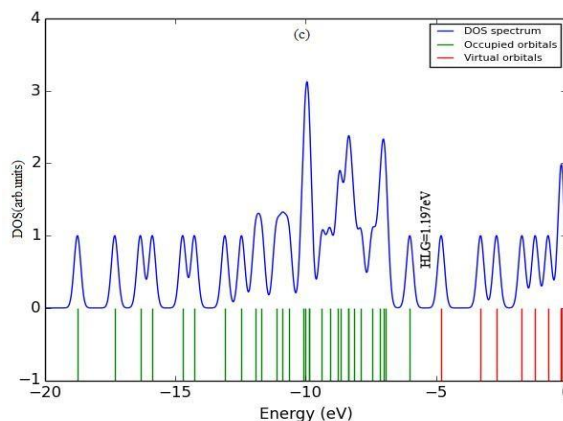
symmetric for the reverse field effect. The HOMO-LUMO gap is getting shifted from 1.904 to 0.272 eV, when the applied electric field is increased from 0 to 0.26 eV.
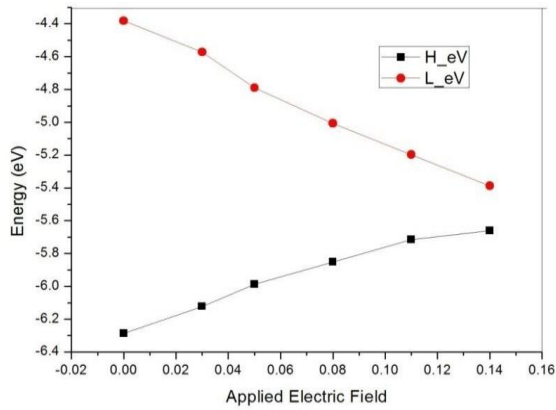

Figure. 8 Showing the variation of HLG of Au and S substituted MMF for the various applied EFs.
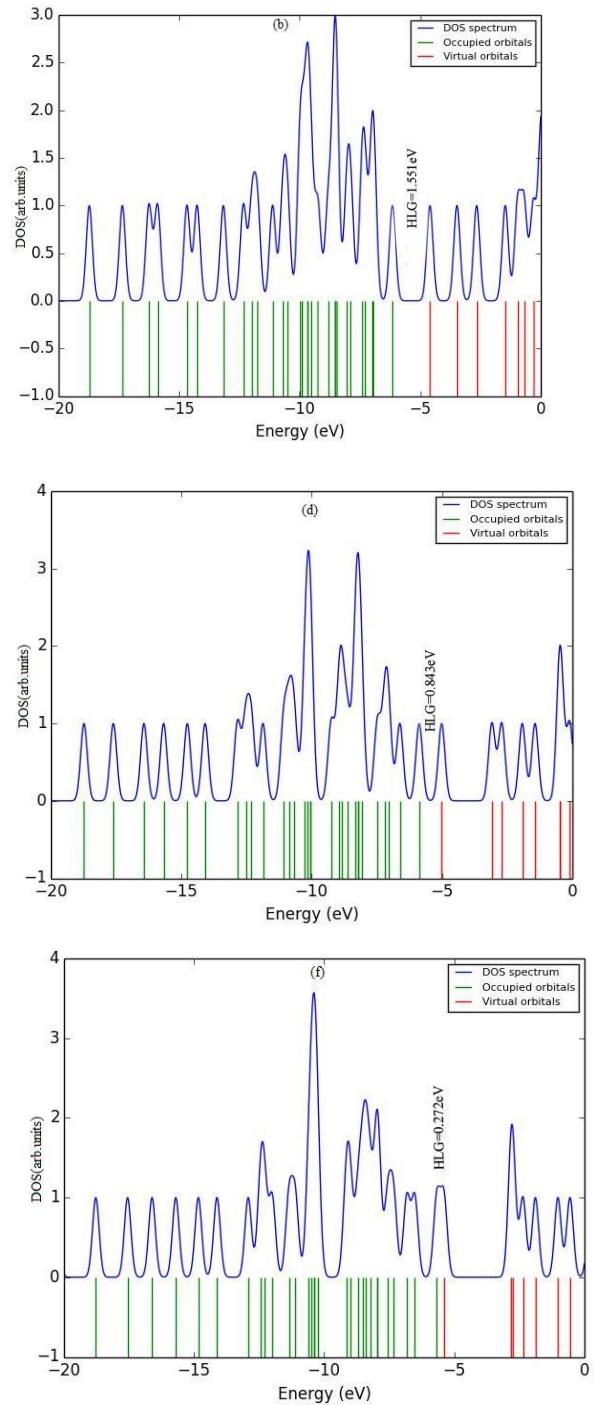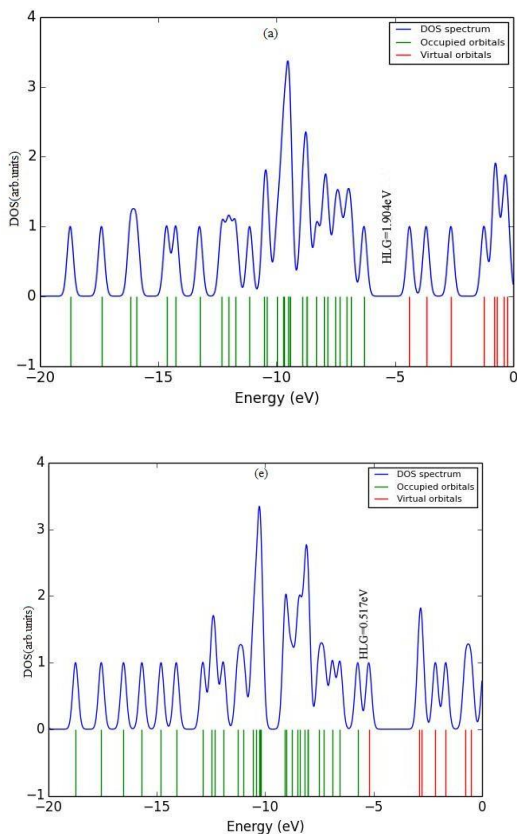

Figure 9. DOS of Au and S substituted MMF for the various applied EFs.

EFs (VÅ^{-1})	HOMO	
0.00		
	Positive field	Negative field
0.05		
0.10		
0.18		
0.21		
0.26		

EFs (VÅ^{-1})	LUMO	
0.00		
	Positive field	Negative field
0.05		
0.10		
0.18		

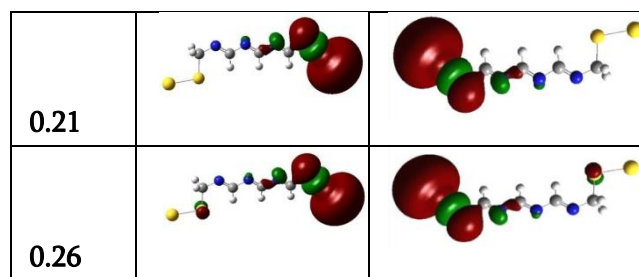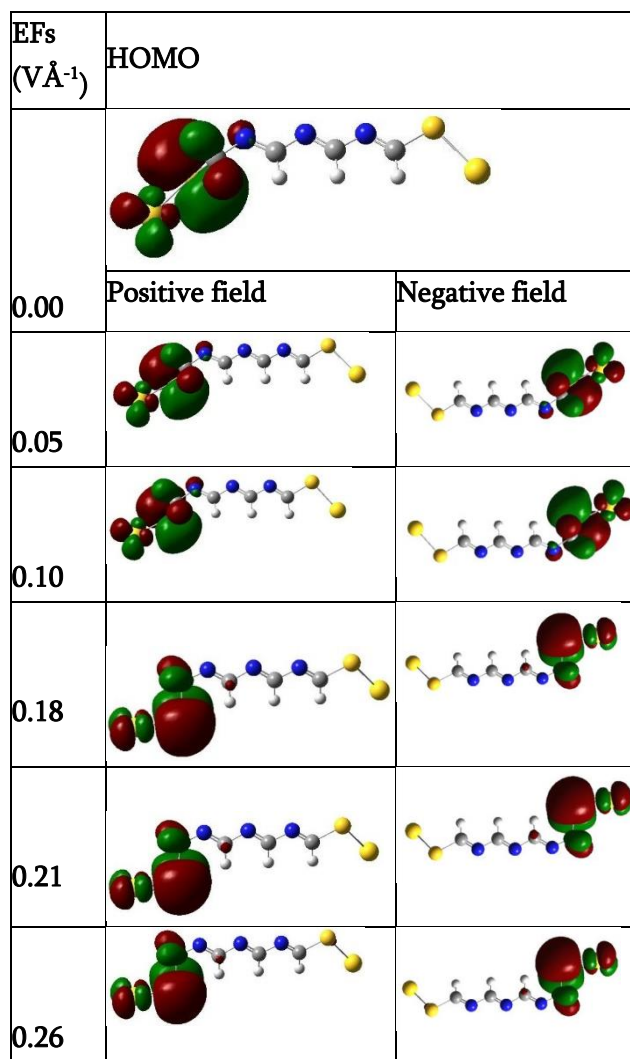| 0.21		
0.26		

Figure 10. The spatial redistribution of the molecular orbitals of Au and S substituted MMF for the zero and various applied EFs, which are drawn at 0.05au surface values.

The density of states (DOS) [24] for the applied bias (0.26 VÅ^{-1}) was depicted in the Fig 9, in which the green solid lines specify the HOMO and the blue shows the LUMO; the decrease of HLG is also shown. The DOS spectrum clearly shows that the hybridization of the molecular level with that of the gold atom expands the DOS peaks. The homo-lumo gap measured from the DOS spectrum is found to be almost equal with the one calculated from Gaussian09 program package. The spatial redistribution of the molecular orbital of the MMF for the zero and higher applied electric fields was shown in the figure 10. For the applied positive electric field, the frontier orbitals are partially localized at the terminals near sulpher and gold atoms and are opposite to each other. When the field direction is reversed, the scenario is extremely symmetric. It is evident that all the atoms of MMF molecule present between the two sulpher atoms are not delocalized. Henceforth, despirt of the small homo-lumo gap, the prospect of the electrical conduction along the Molecular wire is noticed to be very small, thus it behaves like an insulator, which agrees well with the experimental and theoretical reports.

3.6 Molecular Electrostatic Potential

The three dimensional surface picture of electrostatic potential [25] for zero and non-zero field was shown in the figure 11, in which the blue surface depicts the positive potential and red shoes the negative. As
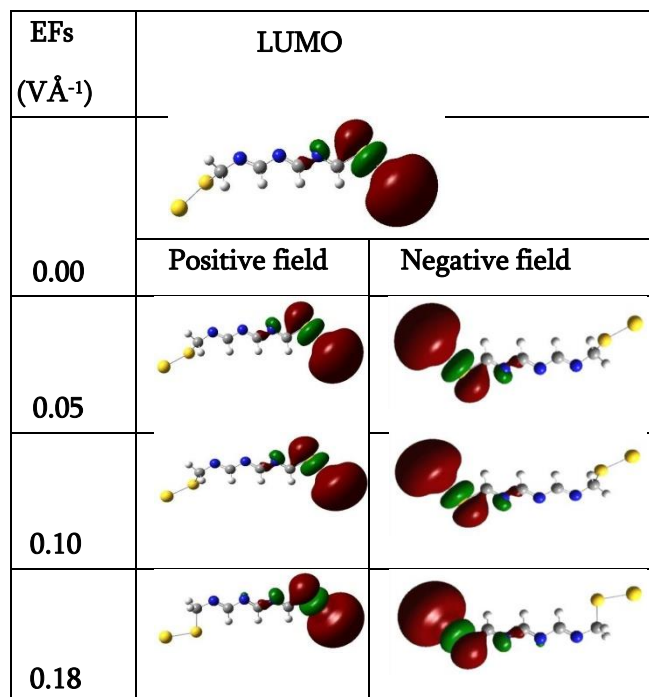
reported in our previous study, the electrostatic potential clearly replicates the opposing influences from the nucleus and electrons, therefore it highly potraited the charged sections of the molecule. The positive surface mounted throughout the backbone of the molecule for the zero applied electric field; this positive influence is qualified from the nuclei. While, the negative potential is pivoted over nitrogen atoms present at right and left ends of the molecule; this situation is nearly even for the field gets escalated from 0 to 0.15 VÅ^{-1}.
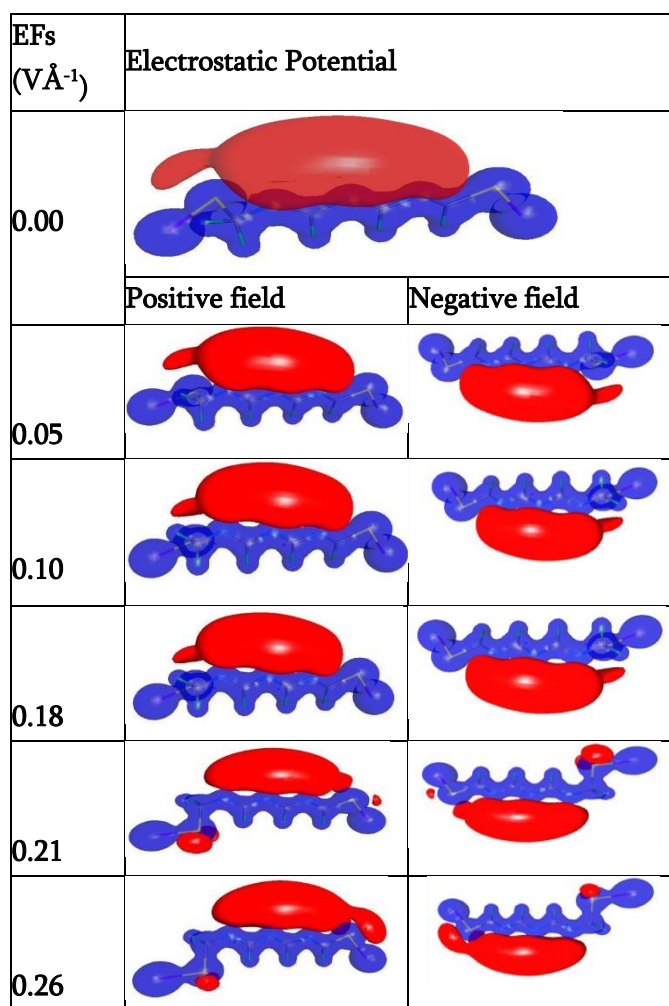
EFs (VÅ^{-1})	Electrostatic Potential	
0.00		
	Positive field	Negative field
0.05		
0.10		
0.18		
0.21		
0.26		

Figure 11. Molecular electrostatic potential of MMF for the different electric potential.

When the field is increased further to 0.21 VÅ^{-1}, the negative electrostatic potential was found to be mounted at the left edge, which gets diluted to a smaller value at 0.26 VÅ^{-1}. In the right end of the

MMF wire, the negative potential is start generating at 0.21 VÅ^{-1} and the potential grows at maximum when the field reaches 0.26 VÅ^{-1}. Likely, the migration of the negative potential is observed from right to left end of the wire, when the field is applied in reverse direction.
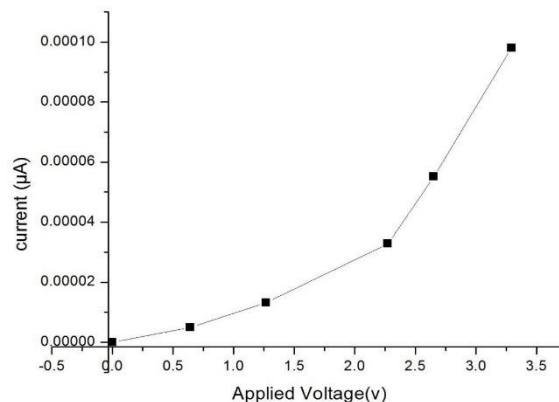
3.7 I-V Relation

Figure 12. I-V characteristics of MMF for the various fields,

The current–voltage (I-V) characteristic curve is normally interpreted to find the basic parameters of electronic devices [26]. The tunneling electric current (I) and the length of the molecular wire L have been calculated for various potential EFs. For all the applied electric fields (E), the bias voltage V across the length of the molecule, L have been calculated from the expression V = EL. Further, using Ohm's law, (I = V/R) [27] the current (I) flows has been calculated for all applied field. Using these parameters, the I–V characteristics of the MMF molecule has been studied. The I-V characterestic plot of MMF shows that, when the bias voltage is raised from 0 eV, the current flow is found to increase gradually showing the nonlinear behavior of the molecule. Since the molecule is symmetric, the characteristic curve is also almost symmetric for both directions of the applied EFs.

3.8 Molecular Polarization

The applied potential polarizes the molecule, which results in change of the dipole moment of the molecule. Hence, it is necessary to find out the dipole moment for all the applied electric field EFs. The variations of molecular dipole moment for the various applied EF were analyzed by Kirtman et al., [28] and found a linear character. Nevertheless, the linearity nature is no longer exists beyond certain potential and it is insignificant as no molecular electronic device works under such high voltages.
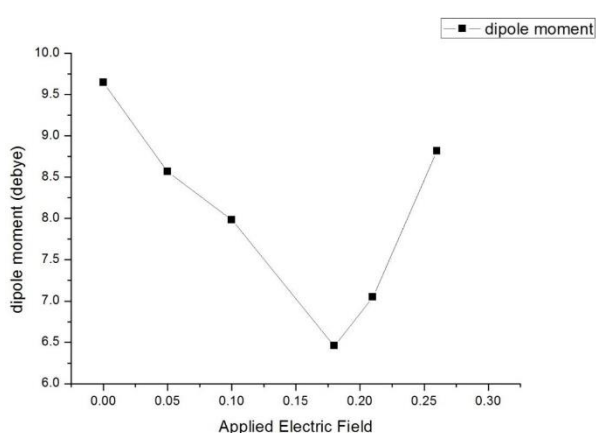

Figure 13. Molecular dipole moment of Au and S substituted MMF at various EFs.

The dipole moment of the molecule has been calculated for all the applied field values. The calculated molecular dipole moment (μ) for 0.05 biases is 8.565 Debye, which decreases almost linearly 6.458 Debye with the increase of field to 0.018 V$Å^{-1}$ then the moment gets linearly increased to 8.817 Debye as the fields' increases to 0.26 V$Å^{-1}$. The molecule found to be highly polarized (9.646 Debye) for the zero field. Fig. 13 shows the variation of x, y and z components of dipole moment (μ_x, μ_y, and μ_z) and the resultant molecular dipole moment (μ) for various applied EFs, the large variation of x-component may be due to the application of field along the x-direction.

IV. CONCLUSION

In the present study, the Au and S substituted MMF molecule has been optimized for the zero and various applied EFs using DFT method by adding polarization and diffuse functions. The significant features of the geometric calculations and electron density analysis of the molecule have been clearly described. The applied field altered the almost all bonds in which the high significant variations were found at Au–S and S–C bond length, which are close to the reported theoretical and experimental values. Surprisingly, when the applied field increases, the Au–S–C–N bonds at both ends are twisted in opposite direction. The bond topological analysis based on the AIM theory shows the difference of charge distribution in all bonds. Further, the redistribution of charges for various applied field are found to be very systematic in the terminal groups especially in the R-end of the wire. The applied electric field appreciably decreases the HOMO-LUMO gap of the molecule from 1.904 eV to 0.272 eV. The spatial redistribution of the frontier orbitals (HOMO and LUMO) shows that all the atoms of MMF molecule between the two thiol atoms are not delocalized. Hence, although the molecular wire exhibit small HLG, there is no possibility of electrical conduction and it acts as an insulating wire. The movement of ESP regions in the ESP map of the molecule for applied potential clearly shows the charged regions and the effect of substitution. This observation gives an insight on this kind of lengthy molecules, which are may be useful to synthesis insulating layers.

V. REFERENCES

[1]. Feng, X.Y., Z. Li, and J. Yang, Electron Transport in Butane Molecular Wires with Different Anchoring Groups Containing N, S and P: A First Principles Study. The Journal of Physical Chemistry C, 2009. 113(52): p. 21911-21914.

[2]. Yu, L.H., C.D. Zangmeister, and J.G. Kushmerick, Structural contributions to charge transport across Ni-octane dithiol multilayer junctions. Nano Lett, 2006. 6(11): p. 2515-9.

[3]. Liu, H., N. Wang, J. Zhao, Y. Guo, X. Yin, Y.C. Boey Freddy, and H. Zhang, Length-Dependent Conductance of Molecular Wires and Contact Resistance in Metal–Molecule–Metal Junctions. Chem Phys Chem, 200, 9(10): p. 1416- 1424.

[4]. Wang, Q., N. Evans, S.M. Zakeeruddin, I. Exnar, and M. Gratzel, Molecular wiring of insulators: charging and discharging electrode materials for high- energy lithium-ion batteries by molecular charge transport layers. J Am Chem Soc, 2007. 129(11): p. 3163-7.

[5]. Bakale, G., W. Tauchert, and W.F. Schmidt, Electron transport in mixtures of liquid methane and ethane. The Journal of Chemical Physics, 1975. 63(10): p. 4470-4473.

[6]. Nogueira, F., A. Castro, and M. Marques, A Tutorial on Density Functional Theory, in A Primer in Density Functional Theory, C. Fiolhais, F. Nogueira, and M. Marques, Editors. 2003, Springer Berlin / Heidelberg. p. 218-256.

[7]. Frisch, M.J., G.W. Trucks, H.B. Schlegel, G.E. Scuseria, M.A. Robb, J.R. Cheeseman, G. Scalmani, V. Barone, G.A. Petersson, H. Nakatsuji, X. Li, M. Caricato, A.V. Marenich, J. Bloino, B.G. Janesko, R. Gomperts, B. Mennucci, H.P. Hratchian, J.V. Ortiz, A.F. Izmaylov, J.L. Sonnenberg, Williams, F. Ding, F. Lipparini, F. Egidi, J. Goings, B. Peng, A. Petrone, T. Henderson, D. Ranasinghe, V.G. Zakrzewski, J. Gao, N. Rega, G. Zheng, W. Liang, M. Hada, M. Ehara, K. Toyota, R. Fukuda, J. Hasegawa, M. Ishida, T. Nakajima, Y. Honda, O. Kitao, H. Nakai, T. Vreven, K. Throssell, J.A. Montgomery Jr., J.E. Peralta, F. Ogliaro, M.J. Bearpark, J.J. Heyd, E.N. Brothers, K.N. Kudin, V.N. Staroverov, T.A. Keith, R. Kobayashi, J. Normand, K. Raghavachari, A.P.

Rendell, J.C. Burant, S.S. Iyengar, J. Tomasi, M. Cossi, J.M. Millam, M. Klene, C. Adamo, R. Cammi, J.W. Ochterski, R.L. Martin, K. Morokuma, O. Farkas, J.B. Foresman, and D.J. Fox, Gaussian 16 Rev. B.01. 2016: Wallingford, CT.

[8]. Lee, C., W. Yang, and R.G. Parr, Development of the Colle-Salvetti correlation-energy formula into a functional of the electron density. Physical Review B, 1988. 37(2): p. 785-789.

[9]. Wadt, W.R. and P.J. Hay, Ab initio effective core potentials for molecular calculations. Potentials for main group elements Na to Bi. The Journal of Chemical Physics, 1985. 82(1): p. 284-298.

[10]. Bader, R., Atoms in Molecules: A Quantum Theory (International Series of Monographs on Chemistry). 1994: Clarendon Press.

[11]. Bader, R.F.W., AIMPAC.

[12]. Volkov, A., T. Koritsanszky, M. Chodkiewicz, and F. King Harry, On the basis- set dependence of local and integrated electron density properties: Application of a new computer program for quantum- chemical density analysis. Journal of Computational Chemistry,2008. 30(9): p. 1379-1391.

[13]. Dennington, R., T.A. Keith, and J.M. Millam, GaussView Version 6. 2016, Wallingford, CT.

[14]. Koritsanszky, T., P. Macchi, C. Gatti, L. Farrugia, P.R. Mallison, A. Volkov, and T. Richter, XD2006. A computer program package for multipole refinement and analysis of charge densities from diffraction data. 2006.

[15]. O'Boyle Noel, M., L. Tenderholt Adam, and M. Langner Karol, cclib: A library for package-independent computational chemistry algorithms. Journal of Computational Chemistry, 2007. 29(5): p. 839-845.

[16]. Burgi, T., Properties of the gold-sulphur interface: from self-assembled monolayers to clusters. Nanoscale, 2015. 7(38): p. 15553-15567.

[17]. Tachibana, M., K. Yoshizawa, A. Ogawa, H. Fujimoto, and R. Hoffmann, Sulfur–Gold Orbital Interactions which Determine the Structure of Alkanethiolate/Au(111) Self-Assembled Monolayer Systems. The Journal of Physical Chemistry B, 2002. 106(49): p. 12727-12736.

[18]. Saffarzadeh, A., F. Demir, and G. Kirczenow, Mechanism of the enhanced conductance of a molecular junction under tensile stress. Physical Review B, 2014. 89(4): p. 045431.

[19]. Eickerling, G., R. Mastalerz, V. Herz, W. Scherer, H.-J. Himmel, and M. Reiher, Relativistic Effects on the Topology of the Electron Density. Journal of Chemical Theory and Computation, 2007. 3(6): p. 2182-2197.

[20]. Jacobsen, H., Chemical bonding in view of electron charge density and kinetic energy density descriptors. Journal of Computational Chemistry, 2008. 30(7): p. 1093-1102.

[21]. Saha, S., K. Roy Ram, and W. Ayers Paul, Are the Hirshfeld and Mulliken population analysis schemes consistent with chemical intuition? International Journal of Quantum Chemistry, 2008. 109(9): p. 1790-1806.

[22]. Reed, A.E., R.B. Weinstock, and F. Weinhold, Natural population analysis. The Journal of Chemical Physics, 1985. 83(2): p. 735-746.

[23]. Reecht, G., C. Lotze, D. Sysoiev, T. Huhn, and K.J. Franke, Visualizing the Role of Molecular Orbitals in Charge Transport through Individual Diarylethene Isomers. ACS Nano, 2016. 10(11): p. 10555-10562.

[24]. McClean, I.P., N. Konofaos, and C.B. Thomas, Conductance technique measurements of the density of states between Si and ZnS grown by molecular beam epitaxy. Journal of Applied Physics, 1993. 74(1): p. 397-401.

[25]. Politzer, P., P.R. Laurence, and K. Jayasuriya, Molecular electrostatic potentials: an effective tool for the elucidation of biochemical phenomena. Environmental Health Perspectives, 1985. 61: p. 191-202.

[26]. Darancet, P., J.R. Widawsky, H.J. Choi, L. Venkataraman, and J.B. Neaton, Quantitative Current–Voltage Characteristics in Molecular Junctions from First Principles. Nano Letters, 2012. 12(12): p. 6250-6254.

[27]. Chapter 2 - Electrochemical and Thermodynamic Fundamentals, in Membrane Science and Technology, H. Strathmann, Editor. 2004, Elsevier. p. 23-88.

[28]. Kirtman, B., S. Bonness, A. Ramirez-Solis, B. Champagne, H. Matsumoto, and H. Sekino, Calculation of electric dipole (hyper)polarizabilities by long- range-correction scheme in density functional theory: A systematic assessment for polydiacetylene and polybutatriene oligomers. The Journal of Chemical Physics, 2008. 128(11): p. 114108.